Chemical Science

Structurally robust phosphorescent [Pt(O^N^C^N)] emitters for high performance organic light-emitting devices with power efficiency up to 126 lm W-1 and external quantum efficiency over 20%

Journal:	*Chemical Science*
Manuscript ID:	SC-EDG-04-2014-001105.R2
Article Type:	Edge Article
Date Submitted by the Author:	26-Jul-2014

Complete List of Authors:
Cheng, Gang; The University of Hong Kong, Chemistry
Kui, Chi Fai; The University of Hong Kong, Chemistry
Ang, Wai-Hung; The University of Hong Kong, Chemistry
Ko, Man-Ying; The University of Hong Kong, Chemistry
KWONG, Chun-Lam; The University of Hong Kong, Chemistry
Kwok, Chi-Chung; The University of Hong Kong, Chemistry
Ma, Chensheng; The University of Hong Kong, Chemistry; The University of Hong Kong, Chemistry
Guan, Xiangguo; The University of Hong Kong, Department of Chemistry
Low, Kam-Hung; GuangDong Aglaia Optoelectronic Materials Co., Ltd.,
Su, Shi-Jian; South China University of Technology, Institute of Polymer Optoelectronic Materials and Devices
Che, Chi-Ming; The University of Hong Kong, Chemistry

Chemical Science

RSCPublishing

EDGE ARTICLE

Structurally robust phosphorescent [Pt(O^N^C^N)] emitters for high performance organic light-emitting devices with power efficiency up to 126 lm W^{-1} and external quantum efficiency over 20%

Cite this: DOI: 10.1039/xoxxoooooox

Received ooth January 2014,
Accepted ooth January 2014

DOI: 10.1039/xoxxoooooox

www.rsc.org/

Gang Cheng,[a,b,d] Steven C. F. Kui,[a,d] Wai-Hung Ang,[a] Man-Ying Ko,[a] Pui-Keong Chow,[a] Chun-Lam Kwong,[a] Chi-Chung Kwok,[a,d] Chensheng Ma,[a,f] Xiangguo Guan,[a] Kam-Hung Low,[e] Shi-Jian Su[c] and Chi-Ming Che*[a,d]

A series of robust, bulky and strongly emissive platinum(II) complexes supported by tetradentate O^N^C^N ligands having *tert*-butyl groups (**1**–**4**) or bridging tertiary amine (**5**) or biphenyl group with spiro linkage (**6**) at the periphery of [O^N^C^N] ligand scaffold have been prepared. Their photophysical properties were examined by absorption and emission spectroscopy, density functional theory calculations, and ultra-fast time-resolved emission measurements. These complexes display emission quantum yields up to 95% with emission maxima λ_{max} in the range of 522 to 570 nm and have a good thermal stability up to T_d > 423 °C. Notably, k_q values of **4**–**6** are in the range of 8.5×10^6 to 2.0×10^7 $mol^{-1} dm^3 s^{-1}$ being smaller than that (~ 10^8 to 10^9 $mol^{-1} dm^3 s^{-1}$) of other reported Pt(II) complexes. The bulky groups at the periphery of [O^N^C^N] ligand disfavour intermolecular interactions and hence excimer formation in solutions. These complexes are good light-emitting material (dopant) for OLEDs since the triplet–triplet annihilation (TTA) and concentration quenching effect arising from intermolecular interactions can be minimized even at high dopant concentration. The efficiency of the devices fabricated with **4**–**6** increased with dopant concentration up to a high level of 10% with no extra emitting component or significant shift in CIE observed. The maximum power efficiency (PE) values achieved for the **5** (yellow-emitting) and **6** (green-emitting) based devices were 118 and 126 lm W^{-1}, respectively. These PE values are the highest among the reported Pt(II)-OLEDs and comparable to that of the best reported Ir(III)-OLEDs without out-coupling technique. Complex **7** is structurally analogous to but less bulky than **3-6**, and is prone to give excimer emission in the solid state. High PE up to 55.5 lm W^{-1} and external quantum efficiency up to 25.1% have been realized in the white OLEDs fabricated with **7** as a single emitting material. These values are compatible to those of the best reported WOLEDs based on a single emitting material.

Introduction

Since the reports on organic electroluminescent devices in 1987[1a] and organic electrophosphorescent devices fabricated with triplet emitters in 1998,[1b,c] there have been continued interests to develop organic light-emitting diodes (OLEDs) as new generation of display and lighting technologies. OLEDs have inherent merits including active luminous, light weight, high efficiency, and low cost. In this area, many phosphorescent metal complexes have been studied as the maximum internal quantum efficiency of OLEDs with phosphorescent emitters could be up to 100% *via* harvesting of both singlet and triplet excitons.[1b,c] Over the past decades, the power efficiency (PE) of green-emitting OLED has been dramatically boosted from 1.5 lm W^{-1} with Alq_3 as emitter in 1987[1a] to 290 lm W^{-1} with $Ir(ppy)_2(acac)$ emitter in 2011,[2] where Alq_3 and $Ir(ppy)_2(acac)$ are tris(8-hydroxyquinolinato) aluminium and bis(2-phenylpyridine)iridium acetylacetonate, respectively.[1a,3b] The latter value of 290 lm W^{-1} is in fact the result of enhanced efficiency of corresponding bottom-emitting OLED (~116 lm W^{-1}) by ~2.5 fold using optical out-coupling technique. In general, Ir(III) complexes[3] are the main stream

light-emitting materials used in phosphorescent OLEDs. Among the bottom-emitting Ir(III)-OLEDs without out-coupling enhancement, the ones based on *fac*-tris(2-phenylpyridine)iridium [Ir(ppy)$_3$][3a] or Ir(ppy)$_2$(acac)[3b] have shown the highest PE up to 133 lm W^{-1}.[2,4] Nonetheless, the stability of blue light-emitting Ir(III) complexes[5a] and structural isomerization issue of cyclometalated [(C^N)-Ir(III)] emitters, both of which would lead to decrease in external quantum efficiency (EQE),[5b] remain to be addressed. In recent years, phosphorescent platinum(II) complexes have been receiving a surge of interests for their applications in material science including the use as phosphorescent dopant in high efficiency OLEDs.[1c,6-10,12-17] By using highly robust, chelating donor ligand(s) coordinated to Pt(II), the efficiency of Pt(II)-OLEDs has been significantly improved and high efficiency Pt(II)-OLEDs with EQE ~20% have been reported.[7] Besides EQE which is the ratio of the number of photons emitted by the OLED into the viewing direction to the number of electrons injected, PE is also an important parameter for practical OLED applications because PE stands for the ratio of luminous power emitted in the forward direction to the total electric power to drive the OLED at a particular voltage.[11] As up to now, the best PE (79.3 lm W^{-1}) of reported green-emitting Pt(II)-OLEDs[7a] is still lower than that of the best reported green-emitting Ir(III)-OLED[4c] by over 50 lm W^{-1}. To achieve high PE, OLEDs should have both high internal quantum efficiency and low driving voltage,[4d] both of which could be addressed by the design of new phosphorescent platinum(II) materials besides the use of new device structure. In some of the reported examples, intermolecular interactions of phosphorescent Pt(II) complexes can be substantially suppressed by using sterically encumbered substituent(s) attached to the periphery of coordinated ligands.[8] For the less bulky phosphorescent platinum(II) complexes in the solid state, both high-energy blue/sky blue light originated from monomer and low-energy yellow-orange light from excimer species[8a,9] could be simultaneously observed. This intriguing spectroscopic feature of luminescent platinum(II) complexes has been harnessed in the design of white OLEDs and white polymer light-emitting diodes (PLEDs) based on one single emitter.[9] To improve the stability and to attain high emission quantum efficiency, we previously reported the use of dianionic tetradentate ligands having strong donor atoms to prepare new phosphorescent platinum(II) complexes. With this approach, a number of thermally stable, phosphorescent Pt(II) complexes that can be prepared *via* a one-pot reaction of Pt(II) salt such as K_2PtCl_4 and tetradentate ligands have been developed.[8,9b,10,12-15] *The one-pot synthesis of structurally robust, strongly luminescent metal emitters with the use of a single multi-dentate chelating ligand is a unique feature of platinum(II) chemistry that is not easily encountered in the coordination chemistry of Ir(III) complexes*.

In previous works, we reported a panel of Pt(II) complexes with the rigid tetradentate [O^N^C^N] (O^N^C^N = 5,5-dibutyl-2-(3-(pyridin-2-yl)-phenyl)-5*H*-indeno[1,2-*b*]pyridin-9-olate or 2-(4-(3,5-di-*tert*-butylphenyl)-6-(3-(pyridin-2-yl)phenyl)pyridin-2-yl)phenolate and their derivatives) ligands that contain fused *6-5-5* and *6-5-6* membered rings (Chart 1).[8,9b] These [Pt(O^N^C^N)] complexes display high emission quantum yields up to 0.90, are thermally stable (T_d > 400 °C), and could be obtained in high purity by sublimation.[8,9b] Among these complexes, **Pt-3** with bulky norbornane group on the periphery of [O^N^C^N] ligand is an excellent green phosphorescent dopant for OLEDs.[8b] The **Pt-3** based green-emitting OLED displayed excellent efficiency and showed low efficiency roll-off (η_L, η_{Ext}(max) = 66.7 cd A^{-1}, 18.2%; η_L, η_{Ext}(1000 cd m^{-2}) = 65.1 cd A^{-1}, 17.7%).

Herein is described a new class of structurally robust phosphorescent Pt(II) complexes supported by the new tetradentate [O^N^C^N] ligands (with fused *6-5-5* and *6-5-6* membered rings, Chart 1) which are functionalized by the incorporation of *tert*-butyl groups (**1**–**4**) or bridging tertiary amine (**5**) or biphenyl group with spiro linkage (**6**) moiety at the periphery of the ligand scaffold. These new [O^N^C^N] ligands are designed in order to enhance the 3D configuration of the Pt(II) complexes, thereby significantly reducing the intermolecular aggregation or excimer formation. Applying the new [Pt(O^N^C^N)] complexes as emitters in simple-structured OLEDs, *high PEs of 118 and 126 lm W^{-1} have been achieved with the respective yellow-emitting **5** and green-emitting **6** devices*. In addition, a high efficiency WOLED was fabricated

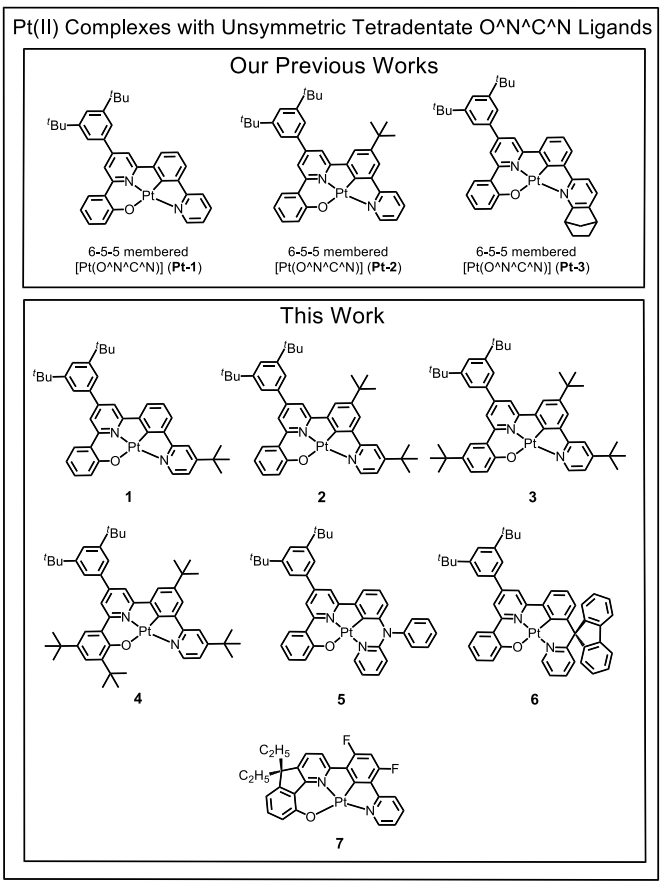

Chart 1 Previously reported Pt(II) complexes with unsymmetric tetradentate O^N^C^N ligands as well as chemical structures of **1–7** in this work.

by using similar device configuration with **7** as a single emitter. Complex **7** is a structurally related but less bulky [Pt(O^N^C^N)] complex that was reported to be strongly phosphorescent and prone to give excimer emission in the solid state. *The maximum EQE and Commission Internationale De L'Eclairage (CIE) coordination for the WOLED fabricated with **7** were 25.1%* and (0.42, 0.46) respectively; *these performance data are compatible to those of the best reported white OLED based on a single emitter.*

Results and discussion

Design and synthesis of ligands and complexes

In previous works, we have reported seven different types of platinum(II) complexes supported by symmetric tetradentate ligands that contain fused (a) *5-5-5* membered metallacycle rings – Prtmen;[12] (b) *6-6-6* membered metallacycle rings – tetra-NHC;[10a,13] and (c) *6-5-6* membered metallacycle rings – N_2O_2 [14] and Salphen;[10b,15] and unsymmetric tetradentate ligands that contain fused (d) *6-5-5* membered metallacycle rings – O^N^C^N [8a,b,9b] and (e) *6-5-6* membered metallacycle rings– O^N^Cab^N [8c] (Chart 2). These aforementioned Pt(II) complexes are thermally stable and display intense phosphorescence in the blue to deep-red spectral region. In literature, Huo and co-workers reported structurally related luminescent [Pt(C^N*N^C)] and [Pt(N^C*C^N)] complexes containing symmetric *5-6-5* membered metallacycle rings.[16a] More recently, Li and co-workers reported Pt7O7,[9c] [Pt(*pmi*-O-CbPy)][7c] and [Pt(ppy-O-popy)][17] complexes containing symmetric *5-6-5* membered rings and unsymmetric *5-6-6* membered rings respectively, some of these complexes have been shown to be highly efficient blue, green and white light-emitting materials (Chart 2).

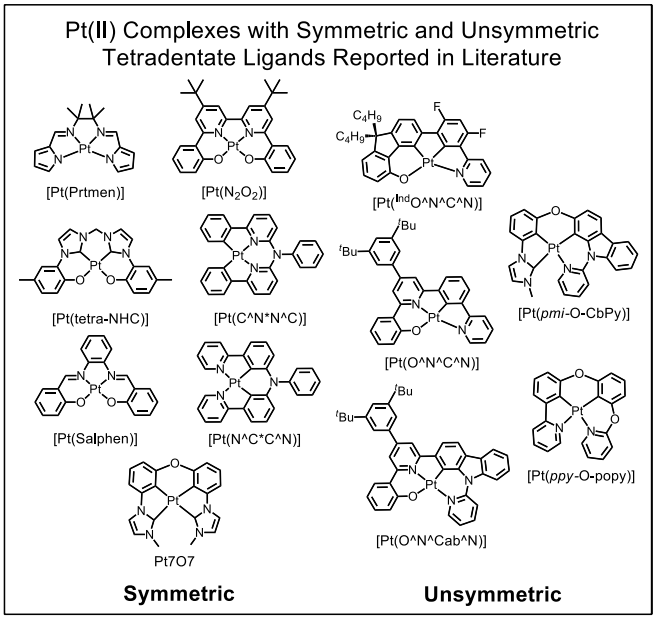

Chart 2 Previously reported Pt(II) complexes with symmetric and unsymmetric tetradentate O^N^C^N ligands reported in literature.

With reference to previous work on **Pt-3** which is an excellent green phosphorescence dopant for OLEDs with low efficiency roll-off, it is conceived that the structure of tetradentate ligand plays a crucial role in phosphorescent platinum(II) complexes to have practical application in OLED.[8b] The ligands should have a bulky encumbered 3D-scaffold so as to retain structural rigidity in order to achieve high thermal stability, minimize non-radiative decay rates and

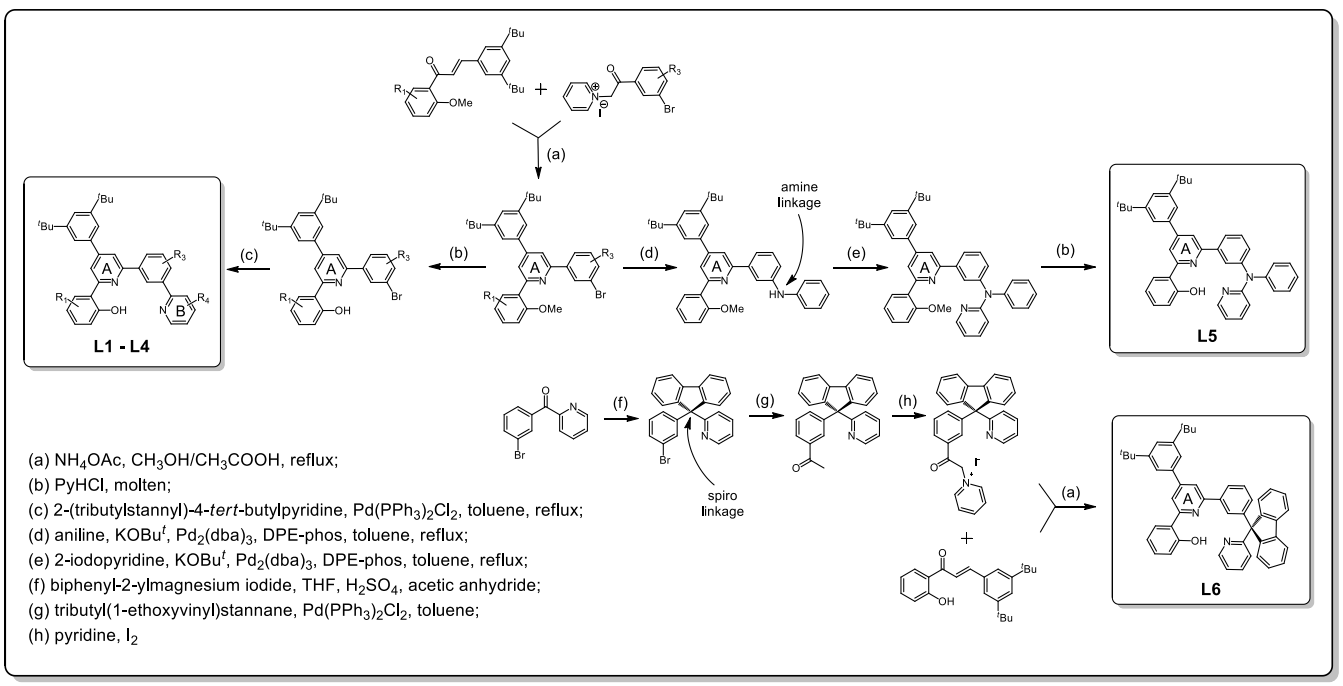

Scheme 1 General synthetic scheme of the new sterically bulky tetradentate O^N^C^N ligands **L1**–**L6**.

suppress intermolecular aggregation or excimer formation of the resultant platinum(II) complexes. With due consideration on the structures of the reported [Pt(O^N^C^N)] complexes, new [O^N^C^N] ligands have been developed in this work by (a) incorporation of *tert*-butyl group(s) at the periphery of the [O^N^C^N] ligands resulting in the Pt(II) complexes **1**–**4** which have *6-5-5* membered metallacycle rings with bulky substituent(s), and (b) putting a bridging tertiary amine or biphenyl group with spiro linkage in between the phenyl group and terminal pyridine group of [O^N^C^N] ligand to give sterically encumbered Pt(II) complexes **5** and **6** both of which contain *6-5-6* membered metallacycle rings.

These new tetradentate [O^N^C^N] ligands **L1–L6** were prepared by the procedures depicted in Scheme 1. Complexes **1–6** were obtained by the reaction of corresponding ligands with K_2PtCl_4 in a refluxing CH_3COOH and $CHCl_3$ mixture (9:1) and were purified by chromatography on SiO_2 column using hexane/ethyl acetate mixture as eluent. The ^1H NMR data of **1**–**6** and all reaction intermediates together with the crystallographic data of **6** are given in the Electronic Supplementary Information (ESI†). Complexes **1**–**6** are air and light stable with T_d up to 423 °C (Table 1). High purity samples of **1**–**6** for OLED fabrication can be obtained by sublimation at around 300 °C under 4×10^{-5} Torr.

The cyclic voltammograms of **1**–**6** in degassed DMF with 0.1 M tetrabutylammonium hexafluorophosphate (TBAP) as supporting electrolyte are given in the ESI† and the electrochemical data are summarized in Table 1. All potentials are referenced to the ferrocenium-ferrocene [$E^0(FeCp_2^{+/0})$] couple. In all cases, there are one irreversible anodic wave with E_{peak} at 0.13–0.47 V and one quasi-reversible cathodic wave with $E_{1/2}$ at −2.13 to −2.22 V. Both the anodic and cathodic waves are attributed to ligand centred oxidation and reduction reactions respectively. This assignment is supported by comparing the cyclic voltammograms of **L6** and **6** (see the ESI†). The HOMO and LUMO levels of these complexes were estimated from the onset oxidation potential and reduction potential at −4.90 to −5.27 eV and −2.40 to −2.67 eV, respectively.

X-ray crystal structure of 6

Perspective view of **6** is depicted in Fig. 1, and crystallographic data of **6** are given in the ESI†. In the crystal structure of **6**, the [Pt(O^N^C^N)] framework is slightly distorted with the torsion angle O-N-C-N of 6.22° being larger than that of **Pt-2** (0.11°) and **Pt-3** (2.55°).[8b] In the crystal structure, the molecules of **6** are aligned in head-to-tail orientation with a Pt···Pt separation of 7.309 Å that is signicantly longer than the values reported in the crystal structures of **Pt-2** (3.218 Å) and **Pt-3** (3.396 Å) having head-to-head orientation alignment of the molecules. The intermolecular π···π distance between each pair of molecules of **6** is about 3.6 Å.

Spectroscopic and photophysical properties

The spectroscopic and photophysical data of **1**–**6** are given in Table 2. As depicted in Fig. 2, these complexes in CH_2Cl_2

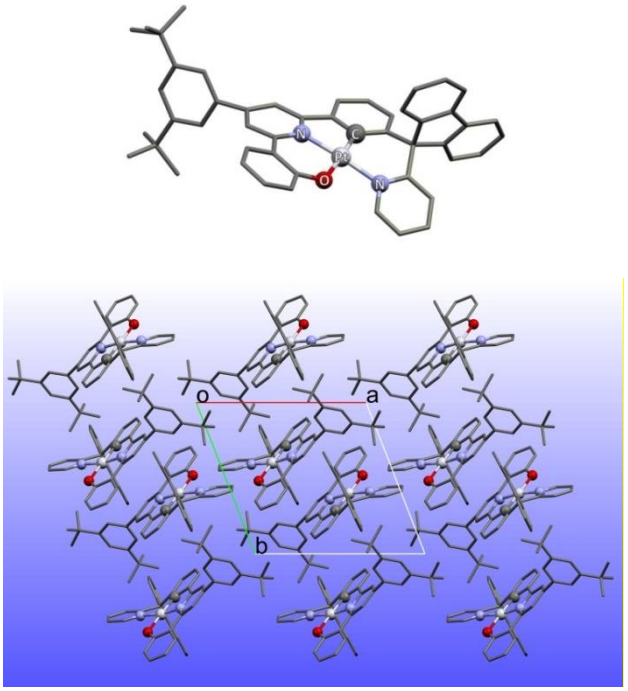

Fig. 1 Perspective view (upper) and molecular packing of **6** viewed along *c*-axis (lower).

display intense absorption bands at wavelength below 300 nm (ε > (4.4–5.0) × 10^4 mol^{-1} dm^3 cm^{-1}), which are assigned to $^1\pi$–π^* transitions of the O^N^C^N ligands, and the moderate intense absorption bands at 430–450 nm (ε ≈ (0.27–0.85) × 10^4 dm^3 mol^{-1} cm^{-1}) with tailing at wavelength beyond 460 nm (ε ≈ 1600–2600 mol^{-1} dm^3 cm^{-1}) that are assigned to transitions with mixed MLCT and IL character. The absorption bands of all of the complexes follow Beer's law at concentrations ranging from 10^{-4} to 10^{-5} mol dm^{-3}. For each of the complexes, the absorption band at around 450 nm displays a small solvatochromic shift (± 5 nm) on changing the solvent from CH_2Cl_2 to toluene, THF, CH_3CN and DMF.

In degassed CH_2Cl_2, complexes **1**–**4** are strongly luminescent with emission quantum yields in the range of 0.23–0.95 and emission lifetimes (τ) in the microsecond time regime (~2.3–5.5 μs) (Table 2). With reference to the spectral data of **Pt-1** and **Pt-2**, the increase in the number of *tert*-butyl groups at the periphery of O^N^C^N ligand causes red-shift of the emission band in the order: 2^{t}Bu (**Pt-1**, λ_{max} = 503 nm) < 3^{t}Bu (**Pt-2**, λ_{max} = 518 nm) ≈ 3^{t}Bu (**1**, λ_{max} = 522 nm) ≈ 4^{t}Bu (**2**, λ_{max} = 522 nm) < 5^{t}Bu (**3**, λ_{max} = 543 nm) < 6^{t}Bu (**4**, λ_{max} = 570 nm) in CH_2Cl_2 solutions (2×10^{-5} mol dm^{-3}). The emission quantum yield of **4** is 0.23, being lower than that of the complexes **Pt-1**, **Pt-2** and **1**–**3** in CH_2Cl_2 solutions. Presumably, the freely rotating *tert*-butyl group at the *ortho*-position of phenolate moiety would promote non-radiative decay of the emissive excited state(s). The red shift of emission peak maximum from 503 nm of **Pt-1** to 551 nm of **5** is attributed to the electron-donating effect of the amine linkage. Meanwhile the emission quantum yield and emission lifetime of **6** are 0.80 and 5.1 μs, respectively, being similar to those values of **Pt-1**,

Table 1 Electrochemical and thermal data of **1**–**6**.

Complex	E_{ox} (V)[a]		E_{red} (V)[a]		HOMO (eV)[b]	LUMO (eV)[b]	E_g (eV)[c]	T_d (°C)[d]
	onset	E_{peak}	onset	$E_{1/2}$				
1	0.13	0.41	-2.13	-2.22	-4.93	-2.67	2.26	402
2	0.14	0.49	-2.22	-2.31	-4.94	-2.58	2.36	356
3	0.26	0.43	-2.16	-2.25	-5.06	-2.64	2.42	371
4	0.25	0.38	-2.18	-2.26	-5.05	-2.62	2.43	391
5	0.33	0.49	-2.14	-2.14	-5.13	-2.66	2.47	423
6	0.47	0.64	-2.17	-2.13	-5.27	-2.63	2.64	412

[a] Determined in DMF at 298 K with 0.1 M tetrabutylammonium hexafluorophosphate (TBAP) as supporting electrolyte; scanning rate: 100 mV s^{-1}. [b] Estimated from onset potentials using $FeCp_2^{+/0}$ values of 4.8 eV below the vacuum level. [c] Electrochemical band gap. [d] Decomposition temperature determined by thermogravimetric analysis.

Table 2 Photophysical data of **Pt-1**, **Pt-2**, **Pt-3** and **1–6**.

Complex	UV-Vis absorption[a] λ_{max}(nm) ($\varepsilon \times 10^4$ (mol^{-1} dm^3 cm^{-1}))	Emission		
		λ_{max}(nm) (τ (μs)) in solution[a]	Φ_{em} in solution; Φ_{em} in film[d]	k_q[e] (mol^{-1} dm^3 s^{-1})
Pt-1	284 (3.8), 371 (1.3), 426 (sh,0.66)	503 (4.7)	0.73[b]	2.1×10^9
Pt-2	285 (4.3), 374 (1.6), 404 (1.0), 438 (sh, 0.72)	518 (3.7)	0.82[b]	1.8×10^9
Pt-3	284 (4.5), 371 (2.1), 421 (sh, 0.94)	522 (4.9)	0.90[b]	8.8×10^7
1	282 (4.5), 372 (1.9), 430 (sh, 0.8)	522 (4.0)	0.77[b]; 0.63	9.0×10^7
2	283 (4.4), 373 (1.6), 435 (sh, 0.69)	522 (4.0)	0.77[b]; 0.58	4.0×10^7
3	286 (4.4), 376 (1.8), 440 (sh, 0.75)	543 (5.5)	0.95[c]; 0.47	8.5×10^6
4	288 (5.2), 376 (2.2), 410 (1.2), 450 (sh, 0.85)	570 (2.3)	0.23[c]; 0.70	9.9×10^6
5	262 (4.4), 278 (4.0), 330 (2.2), 370 (1.1), 450 (sh, 0.27), 481 (sh, 0.21)	551 (4.3)	0.90[c]; 0.74	2.0×10^7
6	261 (5.0), 279 (5.4), 301 (3.6), 329 (1.8), 356 (1.7), 393 (0.72), 431 (sh, 0.38)	517 (5.1)	0.80[b]; 0.91	1.1×10^7

[a] Determined in degassed CH_2Cl_2 (2×10^{-5} mol dm^{-3}). [b] Emission quantum yield was estimated with BPEA (9,10-bis(phenylethynyl)anthracene) in degassed CH_3CN as standard (Φ_{em} = 0.85). [c] Emission quantum yield was estimated with $[Ru(bpy)_2](PF_6)_2$ (bpy = 2,2'-bipyridine) in degassed CH_3CN as standard (Φ_{em} = 0.062). [d] In 2% PMMA film. [e] Self-quenching constant.

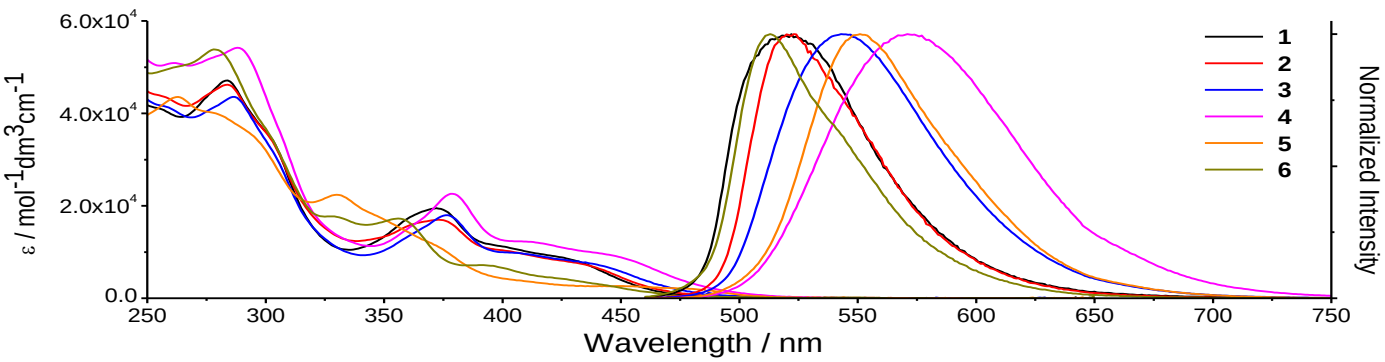

Fig. 2 Absorption and emission spectra of **1**–**6** in CH_2Cl_2 at concentration 2.0×10^{-5} mol dm^{-3}.

Pt-2 and **1**–**2** (Table 2). Similar to the absorption data, the emissions of **1**–**6** display minor solvatochromic effect (*e.g.* λ_{max} of **6** in CH_2Cl_2 at 517 nm is red-shifted to 522 nm in DMF and blue-shifted to 511 nm in toluene). We tentatively assign these emissions to come from excited states having mixed ^{3}MLCT and ^{3}[l→π*(N^C^N)] (l = lone pair of phenoxide) parentage.

Notably, the emission spectra of **3**–**6** reveal no excimer formation in CH_2Cl_2 even at concentration of 1.0×10^{-4} mol dm^{-3}, while excimer emission is observed as a shoulder in the emission spectra of **1**–**2** under similar conditions (Fig. 3). The emission self-quenching rate constants k_q of **1–4** (8.5×10^6 to 9.0×10^7 mol^{-1} dm^3 s^{-1}) are smaller than that of **Pt-1** and **Pt-2** ($(1.8–2.1) \times 10^9$ mol^{-1} dm^3 s^{-1}) and similar to that of **Pt-3** (8.8×10^7). These values are relatively lower than the k_q values (~ 10^8 to 10^9 mol^{-1} dm^3 s^{-1}) of the luminescent Pt(II) complexes reported in the literature. When comparing the effect exerted by the bulky *tert*-butyl substituent in complexes **Pt-1**, **Pt-2** and **1**, the *tert*-butyl group at the terminal pyridine moiety can efficiently block intermolecular interactions resulting in diminished excimer formation in solutions. As the number of *tert*-butyl groups at the periphery of [O^N^C^N] ligand increases, the k_q could be reduced down to 8.5×10^6 mol^{-1} dm^3 s^{-1}. The orthogonal 3D geometry of *N*-phenyl ring of **5** and biphenyl spiro linkage of **6** can effectively suppress intermolecular interactions including the Pt···Pt and/or π···π ones or excimer formation, both of which are the main cause of emission self-quenching of Pt(II) complexes. It is worth noting that the k_q of **5** and **6** can be kept at the level of 2.0×10^7 and 1.1×10^7 mol^{-1} dm^3 s^{-1}, respectively (Table 2).

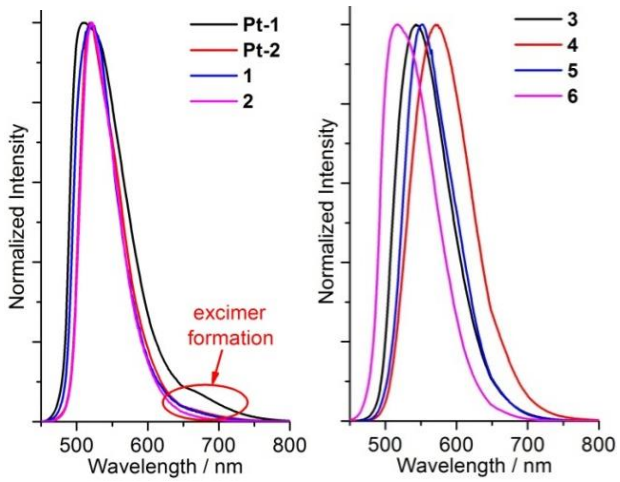

Fig. 3 Emission spectra of **Pt-1**, **Pt-2** and **1**–**6** in CH_2Cl_2 at concentration 1.0×10^{-4} mol dm^{-3}.

DFT calculations and time-resolved emission measurements

Density functional theory (DFT) calculations were performed. The optimized geometries of dimers of **5** and **6** are depicted in Fig. 4. The calculated geometrical parameters are in good agreement with the X-ray crystallography data (Table S1 and Fig. S22 of the ESI†). For example, in the case of **6**, the calculated Pt–N1, Pt–N2, Pt–C, and Pt–O distances are 2.008 Å, 2.064 Å, 1.957 Å, and 2.107 Å while the corresponding bond distances from X-ray crystallography are 2.000 Å, 2.032 Å, 1.950 Å, and 2.049 Å, respectively (Fig. S22). The Pt···Pt distances are 3.916 Å and 4.616 Å for the dimers of **5** and **6**, respectively. These relatively long intermolecular Pt···Pt distances are indicative of insignificant Pt(II)-Pt(II) interactions in the crystal structures of both Pt(II) complexes. Thus, the 3D configuration of the bridging tertiary amine or biphenyl group with spiro linkage can effectively block intermolecular interactions.

TDDFT calculations at M062X/6-311G*(lanl2dz) level based on the geometries of triplet excited states of **5** and **6** gave emission wavelength of 512 nm for **5** and 499 nm for **6**, both of which are in agreement with the experimental data (551 nm (**5**), 517 nm (**6**)). For **5** or **6**, the structural difference between T_1 and S_0 states is small suggesting slow non-radiative decay rate constants (k_{nr}) of T_1 to S_0 in both cases. For both complexes, their HOMO and LUMO are mainly localized on the [O^N^C^N] ligand (Fig. 5). It is interesting to compare the emissive excited states of these two complexes. For **5**, the emission is mainly from HOMO→LUMO (55.3%), and HOMO→LUMO+1 (27.2%), both of which are π-π* transitions localized at the [O^N^C^N] scaffold. As for **6**, the emission is mainly from HOMO-1→LUMO+1 (81.4%), which is mainly attributed to the π-π* transition of the biphenyl substituent at the spiro linkage.

As depicted in Fig. 6, femtosecond time-resolved fluorescence measurements on CH_2Cl_2 solution of **5** or **6** (λ_{ex} = 350 nm) revealed prompt fluorescence that decays with time constant of ~0.44 ps for **5** and 0.15 ps for **6**. This extremely rapid decay of fluorescence suggests the nearly unitary

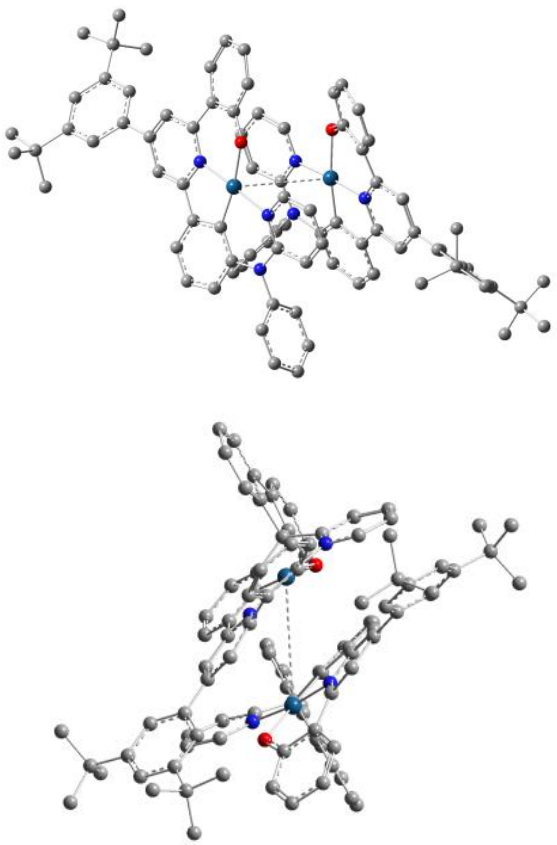

Fig. 4 The optimized geometries of **5** (upper) and **6** (bottom) dimers.

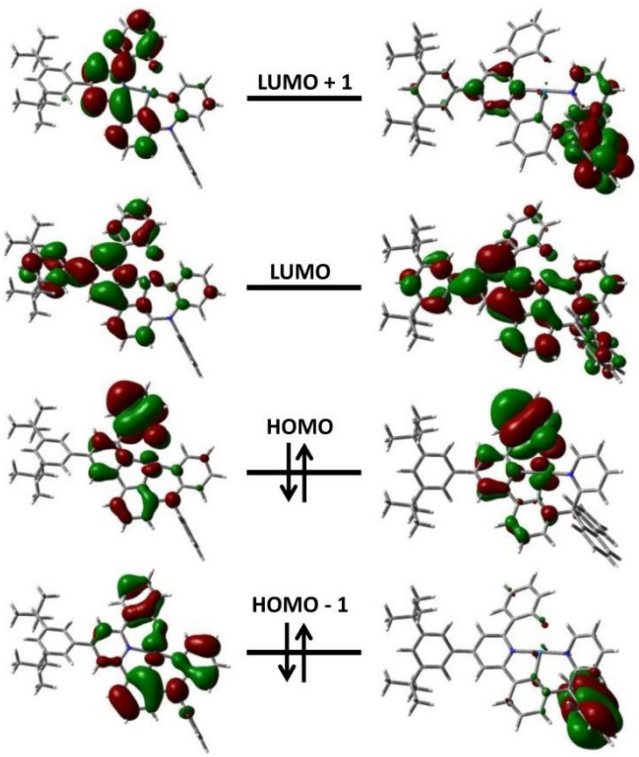

Fig. 5 Frontier MO diagrams of **5** (left) and **6** (right).

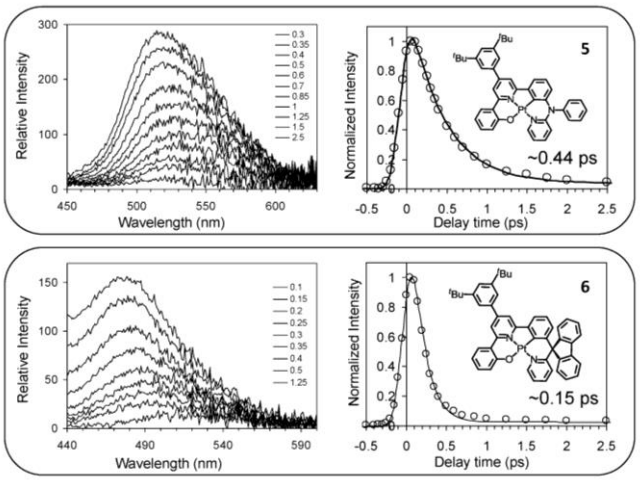

Fig. 6 Time-resolved fluorescence of **5** and **6** in CH_2Cl_2 with excitation at 350 nm.

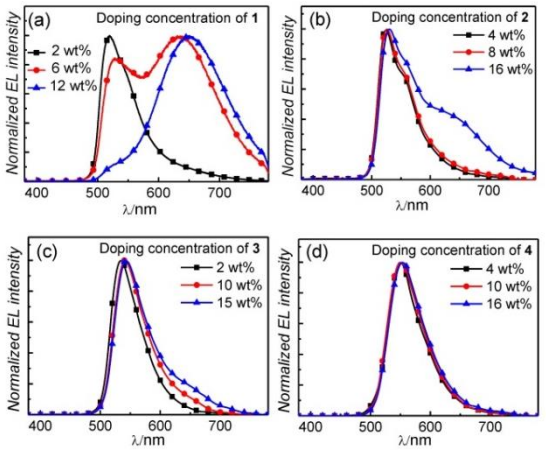

Fig. 7 Normalized EL spectra of OLEDs based on (a) **1**, (b) **2**, (c) **3**, and (d) **4** with different doping concentrations at 1000 cd m^{-2}.

efficiency non-radiative decay attributed to efficient ISC from the electronically excited singlet to give the triplet excited states.[10a,18]

Electroluminescent properties of 1–4

The OLEDs were fabricated with a simple architecture of ITO/MoO_3 (5 nm)/TAPC (50 nm)/TCTA:Pt(II) complex (10 nm)/TmPyPB (50 nm)/LiF (1.2 nm)/Al (150 nm). TAPC (di-[4-(*N*,*N*-ditolyl-amino)-phenyl]cyclohexane) was used as the hole-transporting layer (HTL) while TmPyPB (1,3,5-tri(*m*-pyrid-3-yl-phenyl)) as the electron-transporting layer (ETL).[19] TCTA (4,4′,4″-tris(carbazole-9-yl)triphenylamine) was used as the host material in the emissive layer because of its appropriate highest occupied molecular orbital (HOMO, –5.7 eV) and lowest unoccupied molecular orbital (LUMO, –2.4 eV) levels as well as its high triplet energy level (2.7 eV).[10b]

The EL spectra of OLEDs fabricated with **1**–**4** at different doping concentrations are depicted in Fig. 7. At low doping concentrations, the EL of all devices matched with PL spectra of corresponding Pt(II) emitters measured in solutions (Fig. 2). With increase in doping concentration, the intensity of excimer emission at long wavelength quickly increased for the OLED with **1**. The intensity of the excimer emission was similar to that of the monomer emission for the OLED with 6 wt% **1** while the monomer emission almost vanished for the device with 12 wt% **1**, indicative of the presence of strong intermolecular interactions in the ground and/or excited states of **1**. The dependence of EL spectrum upon doping concentration was weakened for the OLED with **2**; notable excimer emission was only observed at a high complex (dopant) concentration of 16 wt%. The excimer emission was weak for the OLED fabricated with **3** even at high complex concentration of 15 wt% while it was invisible for the device with **4** at 16 wt%. These findings altogether reveal that the intermolecular interactions of both **3** and **4** are weak attributed to the presence of bulky *tert*-butyl groups.

EQE-luminance and PE-luminance characteristics of OLEDs fabricated with **1**–**4** at different doping concentrations

Table 3 Key performances of OLEDs with **1**–**4**.

Complex (C)[a]	L (cd m^{-2})[b]	V (V) at 1[c] cd m^{-2}	V (V) at 10^3 cd m^{-2}	V (V) at 10^4 cd m^{-2}	PE (lm W^{-1})[d] Max.	PE at 10^3 cd m^{-2}	PE at 10^4 cd m^{-2}	CE (cd A^{-1})e Max.	CE at 10^3 cd m^{-2}	CE at 10^4 cd m^{-2}	EQE (%)[f] Max.	EQE at 10^3 cd m^{-2}	EQE at 10^4 cd m^{-2}	CIE (x, y)[g]
1 (2 wt%)	22000	2.7	4.9	7.9	92.0	52.5	21.8	83.4	81.1	55.0	24.4	24.0	16.4	(0.32, 0.63)
1 (6 wt%)	12000	2.7	5.9	10.0	25.2	13.4	5.2	25.5	24.9	16.4	13.5	13.0	8.6	(0.48, 0.50)
1 (12 wt%)	5500	2.8	7.1	12.5	6.7	4.4	1.3	11.1	10.0	5.3	10.9	9.9	5.2	(0.60, 0.40)
2 (4 wt%)	13400	2.9	5.5	9.3	61.5	32.2	10.5	68.3	56.4	31.4	19.7	15.4	8.6	(0.34, 0.62)
2 (8 wt%)	18600	2.9	5.4	8.6	60.0	41.8	16.8	75.0	71.0	46.6	20.6	19.5	13.1	(0.35, 0.62)
2 (16 wt%)	26100	2.8	5.4	8.4	48.6	28.3	16.1	51.0	49.3	43.4	20.4	19.6	17.1	(0.42, 0.56)
3 (2 wt%)	21800	2.9	4.6	7.2	98.1	55.4	20.0	93.7	82.2	46.0	23.8	20.7	11.2	(0.39, 0.60)
3 (10 wt%)	66000	2.8	4.5	6.7	94.3	58.2	32.1	90.0	84.0	68.1	24.8	23.2	18.8	(0.39, 0.60)
3 (15 wt%)	70200	2.8	4.7	7.0	65.3	44.1	23.2	72.7	66.9	51.2	21.8	20.1	15.4	(0.40, 0.58)
4 (4 wt%)	11600	3.1	5.7	9.7	82.1	33.5	7.4	86.1	61.1	22.8	22.7	16.0	6.6	(0.41, 0.57)
4 (10 wt%)	29000	3.0	4.8	7.5	86.4	64.8	26.5	100.5	99.7	62.8	27.1	26.8	16.8	(0.41, 0.57)
4 (16 wt%)	28000	2.9	4.8	7.0	91.0	60.6	32.6	94.0	92.3	73.8	26.3	25.4	19.1	(0.43, 0.56)

[a] Doping concentration. [b] Luminance at 10.5 V. [c] Turn-on voltage (V_{on}). [d] Power efficiency. [e] Current efficiency. [f] External quantum efficiency. [g] CIE coordinates at 1000 cd m^{-2}.

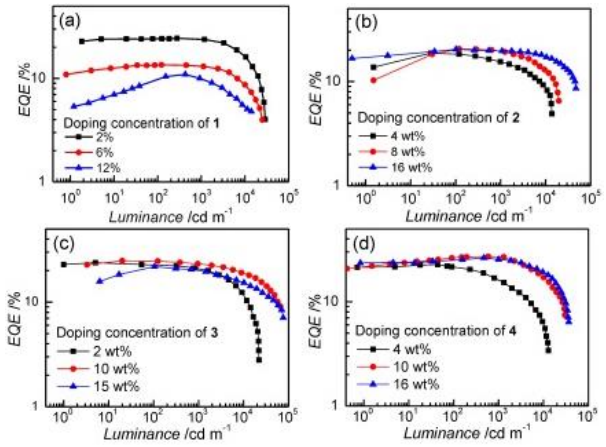

Fig. 8 External quantum efficiency-luminance characteristics of OLEDs fabricated with (a) **1**, (b) **2**, (c) **3**, and (d) **4** at different doping concentrations.

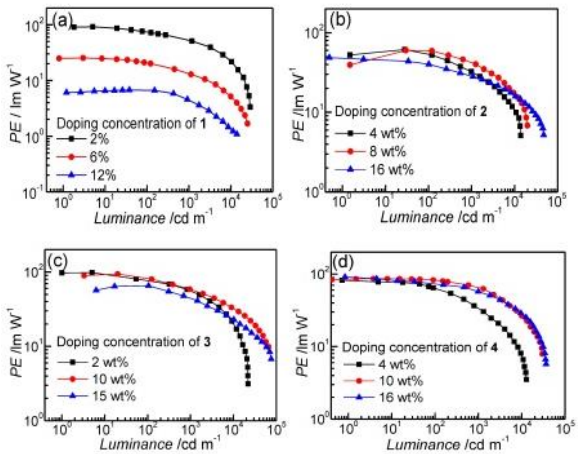

Fig. 9 Power efficiency-luminance characteristics of OLEDs based on (a) **1**, (b) **2**, (c) **3**, and (d) **4** with different doping concentrations.

are depicted in Figs. 8 and 9, respectively, and the corresponding EL performances are listed in Table 3. Maximum PE of 92.0 lm W^{-1} has been achieved for the device with 2 wt% **1**. Maximum EQE of 27.1% has been achieved for the device with 10 wt% **4**, and this value slightly dropped to 26.8% and 16.8% at high luminance of 1000 cd m^{-2} and 10000 cd m^{-2}, respectively. The optimized external quantum efficiencies of the devices fabricated with **1** and **4** are both higher than that of the devices fabricated with **2** and **3**. This is in line with the findings on thin film quantum efficiency of the metal complexes being in the order of **1** ≈ **4** > **2** ≈ **3** (Table 2).

Electroluminescent properties of 5 and 6

The OLEDs were constructed with the device architecture as follows: **5** or **6**; ITO/MoO_3 (5 nm)/HTL (50 nm)/TCTA:Pt(II) complex (10 nm)/ETL(50 nm)/LiF (1.2 nm)/Al (150 nm). TAPC was used as the HTL while TmPyPB or Tm3PyBPZ (2,4,6-tris(3-(3-(pyridin-3-yl)phenyl)phenyl)-1,3,5-triazine) as the ETL. The EL spectra of OLEDs fabricated with **5** or **6** at doping concentrations ranging from 2 to 30 wt% are depicted in

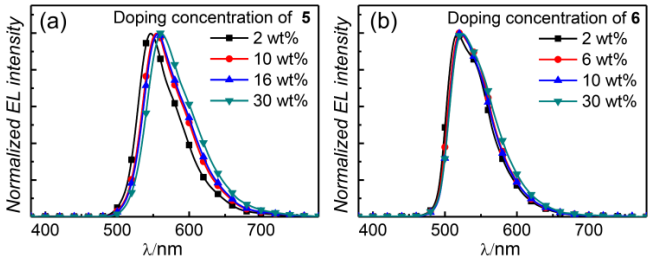

Fig. 10 Normalized EL spectra of OLEDs based on (a) **5** and (b) **6** with different doping concentrations at 1000 cd m^{-2}.

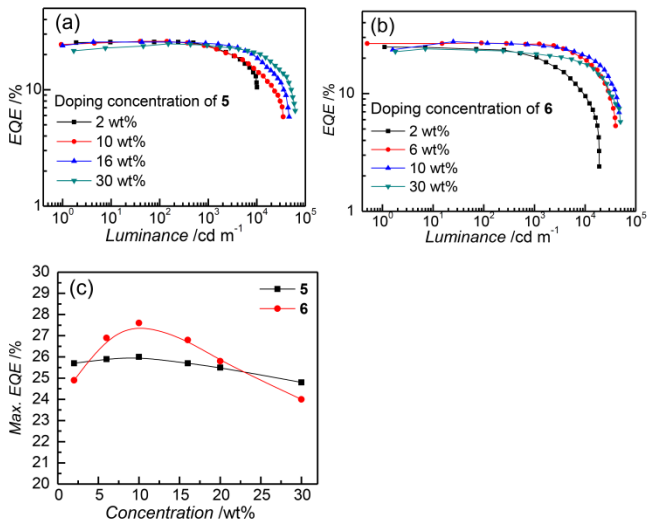

Fig. 11 External quantum efficiency-luminance characteristics of OLEDs based on (a) **5** and (b) **6** with different doping concentrations. (c) Maximum EQE versus doping concentration of OLEDs based on **5** and **6**.

Fig. 10a and Fig. 10b respectively. TmPyPb was used as the ETL in these devices (TmPyPb-devices). At low dopant concentration of 2 wt%, both EL emissions were identical to the corresponding PL emission measured in solutions (Fig. 2), revealing that the EL was originated from the Pt(II) complex in both devices. With increase in the concentration of Pt(II) complex, red-shift of EL maximum from ~550 nm at 2 wt% to ~560 nm at 30 wt% was observed in the case of **5**-device, whereas such red-shift of EL was hardly observed in the case of the **6**-device. This could be rationalized by the more favourable intermolecular interactions in the case of **5** than that of **6**. As discussed in the previous section, the intermolecular interactions are weak for both Pt(II) complexes. Nevertheless, the relatively smaller Pt···Pt distance of **5** dimer may contribute to the notable red-shift of EL maximum of the **5**-device depicted in Fig. 10a.

Fig. 11a and Fig. 11b depict the respective EQE-luminance characteristics of TmPyPb-OLEDs fabricated with **5** or **6** at different doping concentrations. Current density-luminance-voltage and power efficiency-luminance properties are given in Fig. S27 and Fig. S28 of the ESI†. *Maximum EQE of 27.6%, current efficiency of 104.2 cd A^{-1}, and PE of 109.4 lm W^{-1} have been achieved for the TmPyPb-OLED having 10 wt% **6**.*

*Similarly, high maximum EQE of 26.0%, current efficiency of 100.0 cd A^{-1} and PE of 105.5 lm W^{-1} have been achieved with the TmPyPb-OLED having 10 wt% **5*** (Table 4). At high luminance of 1000 cd m^{-2}, EQEs of OLEDs with 10 wt% **5** and 10 wt% **6** slightly dropped to 23.1% and 25.6%, respectively. At very high luminance of 10000 cd m^{-2}, the EQE remained at 20% for the TmPyPb-OLED with 10 wt% **6**. As mentioned in the previous section, complexes **5** and **6** display slow non-radiative decay rate constants (k_{nr}) of T_1 to S_0 as well as the efficient ISC from the electronically excited singlet to triplet states, thereby accounting for the high efficiency and low efficiency roll-off of TmPyPb-OLEDs fabricated with these two complexes.

Fig. 11c depicts the dependence of maximum EQE on the doping concentration of TmPyPb-OLEDs with dopant **5** or **6** as the emitting material. The maximum EQE of the **6** device increased with concentration of dopant from 24.9% at 2 wt% to 27.6% at 10 wt% and then decreased to 24% at 30 wt%. Whereas, the maximum EQE of the **5** device was less sensitive to the concentration of dopant, being 25.7% at 2 wt%, 26.0% at 10 wt% (highest value), and 24.8% at 30 wt%. This could be rationalized by the different emission origins aforementioned in TDDFT calculations; the emission of **5** is mainly from π-π* transitions of the O^N^C^N ligand scaffold and that of **6** mainly from π-π* transitions of the biphenyl substituent at the spiro linkage. Thus, the EL of **5** is envisioned to be less sensitive to the intermolecular interaction and hence the concentration of platinum(II) complex (dopant).

To further enhance the PE of OLEDs fabricated with **5** or **6**, TmPyPb was replaced by Tm3PyBPZ as the ETL and Tm3PyBPZ-OLEDs were fabricated. For the Ir(ppy)$_3$-based OLEDs, such a change in ETL could decrease the driving voltage and thereby increase the PE of OLEDs due to the lower-lying LUMO level of Tm3PyBPZ.[19] As listed in Table 4 and depicted in Fig. S29 and Fig. S30 of the ESI†, the turn-on voltage of Tm3PyBPZ-OLEDs was lower than that of TmPyPb-OLEDs fabricated with **5** or **6** by ~0.4 V at the same doping concentration. Therefore, as depicted in Fig. 12, *the maximum PEs have been improved to 118 and 126 lm W^{-1} for the **5**- and **6**-devices, respectively*. *To our best knowledge, these values are the highest among the reported Pt(II)-OLEDs*[6-10,12-17] *and comparable to that of the best reported Ir(III)-OLEDs without out-coupling enhancement.*[4] The maximum EQE of Tm3PyBPZ-OLED was slightly lower than that of TmPyPb-OLED but with higher efficiency roll-off. This could be the result of the lower triplet energy level of Tm3PyBPZ, which may less efficiently confine triplet excitons in the EML.

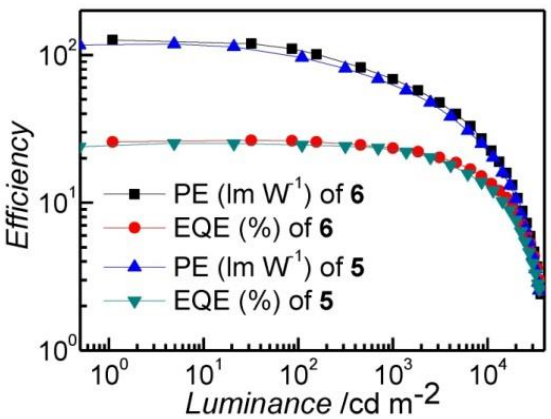

Fig. 12 Power efficiency-external quantum efficiency-luminance characteristics of OLEDs with the structure of ITO/MoO$_3$/TAPC/TCTA:**5** or **6** (10 wt%)/Tm3PyBPZ/LiF/Al.

Electroluminescent properties of 7

In addition to the newly developed **1–6**, we also used the reported [Pt(O^N^C^N)] (**7**),[9b] as a single emitter to fabricate white OLED. Complex **7** was firstly reported and used as a single emitter in white PLEDs by our group. White light with EQE of 11.51%, CIE coordinates of (0.41, 0.45), and CRI of 74 at 1000 cd m^{-2} has been observed from the optimized PLED with concentration of **7** (dopant) at 16 wt%.[9b] To improve the EQE and PE of the white OLED with **7** as a single emitter, devices with an architecture of ITO/MoO$_3$ (5 nm)/TAPC (50 nm)/host: 7 wt% **7** (10 nm)/EML (50 nm)/LiF (1.2 nm)/Al (150 nm) were fabricated and characterized. In these devices, 26DCzppy or TCTA/26DCzppy (1:1 in weight) was used as single host (SH) or double host (DH) while TmPyPb or Tm3PyBPZ was used as the ETL. 26DCzppy was an appropriate host material for **7** and high EQE of 25.1% has been achieved in the SH/TmPyPb device (SH = 26DCzppy) at low luminance. Upon increase of luminance, EQE of the SH/TmPyPb device slightly dropped to 22.6% at 100 cd m^{-2} and 17.2% at 1000 cd m^{-2} as depicted in Fig. 13a and Table 5. As the driving voltage of this device was relatively high (V_{on} = 3.5 V), improvement on its PE was made *via* decreasing its driving voltage. For OLEDs with **1**–**6**, in which TCTA was used as the host, their V_{on} (~2.8 V) was much lower, indicating that the usage of TCTA as the host material could effectively

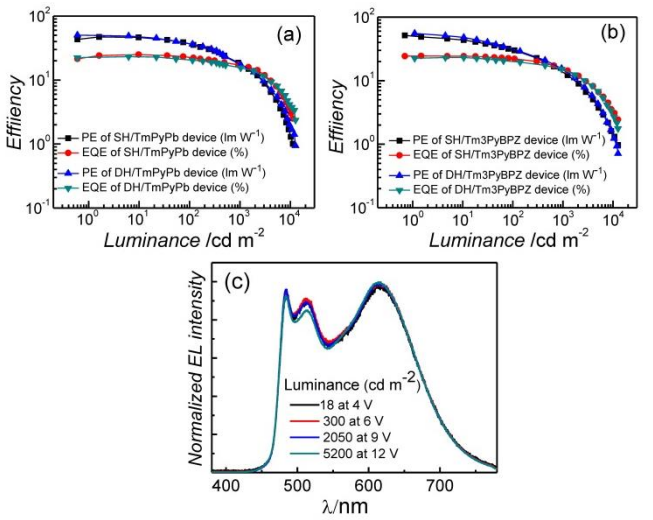

Fig. 13 EQE-PE-luminance characteristics of white OLEDs with **7** as the single emitter; (a) 26DCzppy as single host (SH) or TCTA/26Dczppy = 1:1 as double host (DH) and TmPyPb as ETL; (b) 26DCzppy as single host (SH) or TCTA/ 26Dczppy = 1:1 as double host (DH) and Tm3PyBPZ as ETL. (c) Normalized EL spectra of the DH/Tm3PyBPZ device at different luminance.

Table 4 Key performances of OLEDs with **5** and **6**.

Complex (C)[a]	L (cd m^{-2})[b]	V (V) at 1[c] cd m^{-2}	V (V) at 10^3 cd m^{-2}	V (V) at 10^4 cd m^{-2}	PE (lm W^{-1})[d] Max.	PE (lm W^{-1})[d] at 10^3 cd m^{-2}	PE (lm W^{-1})[d] at 10^4 cd m^{-2}	CE (cd A^{-1})[e] Max.	CE (cd A^{-1})[e] at 10^3 cd m^{-2}	CE (cd A^{-1})[e] at 10^4 cd m^{-2}	EQE (%)[f] Max.	EQE (%)[f] at 10^3 cd m^{-2}	EQE (%)[f] at 10^4 cd m^{-2}	CIE (x, y)[g]
5 (2 wt%)[h]	10100	2.9	5.1	9.5	103.0	54.7	12.8	96.3	88.4	40.2	25.7	23.3	11.4	(0.42, 0.57)
5 (10 wt%)[h]	33400	2.8	5.1	8.3	105.5	54.7	20.6	100.0	88.9	55.4	26.0	23.1	14.4	(0.44, 0.55)
5 (16 wt%)[h]	40000	2.8	5.0	8.0	101.3	57.9	27.7	96.8	94.2	70.4	25.7	24.0	18.7	(0.45, 0.54)
5 (30 wt%)[h]	51200	2.8	5.0	7.7	80.7	50.1	27.8	82.5	80.0	68.4	24.8	24.3	20.5	(0.47, 0.52)
6 (2 wt%)[h]	19000	2.9	5.0	8.5	99.6	48.3	12.6	91.7	75.3	34.7	24.9	20.4	9.59	(0.29, 0.64)
6 (6 wt%)[h]	40000	2.8	4.8	7.4	106.7	65.1	31.1	101.1	98.8	73.1	26.9	26.2	19.1	(0.31, 0.64)
6 (10 wt%)[h]	47000	2.7	4.7	7.2	109.4	65.3	24.7	104.2	98.1	79.2	27.6	25.6	20.0	(0.31, 0.64)
6 (30 wt%)[h]	49700	2.7	4.9	7.4	95.7	52.3	28.4	90.0	82.2	66.9	24.0	21.9	17.9	(0.33, 0.63)
5 (10 wt%)[i]	35000	2.4	4.3	6.2	118.0	62.1	22.5	94.3	84.4	48.0	25.3	22.7	12.5	(0.44, 0.55)
6 (10 wt%)[i]	35300	2.4	4.0	6.1	126.0	68.2	24.4	98.8	87.6	52.0	26.4	23.4	13.6	(0.31, 0.63)

[a] Doping concentration. [b] Luminance at 10 V. [c] Turn-on voltage (V_{on}). [d] Power efficiency. [e] Current efficnecy. [f] External quantum efficiency. [g] CIE coordinates at 1000 cd m^{-2}. [h] TmPyPb is used as the ETL. [i] Tm3PyBPZ is used as the ETL.

Table 5 Key performances of white OLEDs with **7** having different device structures.

Device type	L[a] (cd m^{-2})	V_{on}[b] (V)	PE (lm W^{-1})[c] Max.	PE (lm W^{-1})[c] at 10^2 cd m^{-2}	PE (lm W^{-1})[c] at 10^3 cd m^{-2}	CE (lm W^{-1})[d] Max.	CE (lm W^{-1})[d] at 10^2 cd m^{-2}	CE (lm W^{-1})[d] at 10^3 cd m^{-2}	EQE (%)[e] Max.	EQE (%)[e] at 10^2 cd m^{-2}	EQE (%)[e] at 10^3 cd m^{-2}	CIE (x, y)[f]	CRI
SH[g]/TmPyPb	11200	3.5	47.1	36.7	17.8	56.0	50.6	37.9	25.1	22.6	17.2	(0.38, 0.47)	69
DH[h]/TmPyPb	12700	3.0	50.3	36.8	17.6	49.6	44.2	33.4	23.2	20.8	15.5	(0.41, 0.46)	76
SH[g]/Tm3PyBPZ	12600	3.2	51.5	30.2	13.4	52.9	48.0	32.8	24.5	22.2	15.9	(0.41, 0.47)	76
DH[h]/Tm3PyBPZ	13000	2.7	55.5	31.0	15.0	48.8	42.2	31.5	23.0	20.2	15.1	(0.42, 0.46)	78

[a] Max. luminance. [b] Turn-on voltage: the driving voltage at luminance ~1 cd m^{-2}. [c] Power efficiency. [d] Current efficiency. [e] External quantum efficiency. [f] CIE coordinates at 1000 cd m^{-2}. [g] Single host (SH) material (26DCzppy) is used. [h] Double host (DH) materials (TCTA/26DCzppy = 1:1) are used.

lower the driving voltage. As depicted in Fig. S31 (ESI†), when the 26DCzppy host was replaced by TCTA in the SH/TmPyPb device, V_{on} was decreased to 2.8 V. However, EQE (20.9%) of the TCTA device was relatively lower. By combining 26DCzppy and TCTA with weight ratio of 1:1 as a DH, V_{on} of the DH/TmPyPb device has been effectively decreased to 3.0 V and its EQE was kept at a high level of 23.2%. According to the results of OLEDs with **5** and **6**, the replacement of TmPyPb by Tm3PyBPZ as the ETL could further lower V_{on}. As depicted in Fig. 13b and Table 5, V_{on} has been further decreased to 2.7 V for the DH/Tm3PyBPZ device and PE of this device was as high as 55.5 lm W^{-1}. These values are compatible to the best reported white OLED based on a single emitter.[9a,c] In addition, CIE coordinates of (0.42, 0.46) and colour rendering index (CRI) of 78 at 1000 cd m^{-2} (Table 5) have been achieved in the DH/Tm3PyBPZ device and the corresponding EL spectrum was stable with increased luminance (Fig. 13c). Preliminary study on the operational stability of the white OLED with **7** as emitter was undertaken by using a known stable but less efficient device structure of ITO/MoO_3 (5 nm)/NPB (70 nm)/TCTA (10 nm)/mCBP: 6 wt% **7** (40 nm)/BAlq (40 nm)/LiF (1.2 nm)/Al (150 nm).[9c] The dependence of relative luminance upon operation time of the white OLED operated at a constant current density of 1 mA cm^{-2} with an initial luminance of 1630 cd m^{-2} is depicted in Fig. S33a (ESI†). From the preliminary study on the operational stability of this white OLED device, the lifetime at 50% initial luminance (LT_{50}) was 116.4 h as depicted in Fig. S33a (ESI†). With the formula $LT_{50}(L_1) = LT_{50}(L_0) \times (L_0/L_1)^{1.7}$,[9c,24] where L_1 and L_0 respectively represent the objective and experimental (1630 cd m^{-2}, here) initial luminance, LT_{50} at an objective luminance of 100 cd m^{-2} could be 13386 h. This value is comparable to the value of over 10000 h reported by G. Li *et al.* on white OLEDs fabricated with single Pt(II) emitter.[9c]

General remark

The square-planar coordination geometry of Pt(II) complexes facilitates axial intermolecular interactions that drive the formation of aggregates in the ground state and in the excited state. Although intermolecular aggregation and/or excimer formation can be used to develop single-doped WOLED, this characteristic feature of Pt(II) complexes could result in emission self-quenching at high complex concentration thereby leading to efficiency roll-off due to triplet-triplet annihilation (TTA) process in OLED. Therefore, the colour purity, device efficiency, efficiency roll-off at high luminance and lifetime of OLED could be significantly affected at high doping concentration of phosphorescent Pt(II) emitter, which is detrimental for the application of Pt(II)-emitting materials in the RGB panel.[20,21]

TTA is an important factor governing efficiency roll-off in phosphorescent OLEDs. In principle, triplet excitons can move

towards each other through Dexter energy transfer *via* exchange interactions. TTA can only occur if two triplet excitons are in close proximity and would be enhanced in highly concentrated host-guest systems. To obtain OLED with high brightness, the doping concentration of phosphorescent metal complex must achieve a reasonable high level in order to fully utilize the excitons generated. But at the same time, TTA could be introduced at high concentration of dopant that leads to serious efficiency roll-off.[20]

Therefore, the average distance between emitter molecules should be as large as possible and the aggregation should be prevented in order to minimize the aforementioned Dexter-based TTA. One effective strategy is to install rigid and bulky substituent(s) so as to disfavour intermolecular interactions. In this work, we demonstrated that the incorporation of *tert*-butyl groups (**1**–**4**), bridging tertiary amine unit (**5**), biphenyl group with spiro linkage (**6**) to the ligand scaffold of Pt(II) complexes is an effective strategy to give OLED emitters with high emission quantum yields and diminished efficiency roll-off behaviour. The findings of this work revealed that complexes **5** and **6** display insignificant intermolecular interactions when compared to **1**–**4**. The orthogonal bridging tertiary amine unit [16] or biphenyl group with spiro linkage [22,23] can efficiently suppress intermolecular interactions and further minimize the Dexter-based TTA. Furthermore, the cross-shaped molecular structure of **5** or **6** would cause entanglement in the amorphous state thereby disfavours recrystallization in the emissive layer of OLED.

Complexes **5** and **6** are good candidate materials for PHOLED as they have (i) high emission quantum yield (ϕ = 0.8–0.9), (ii) rigid structure for restricting intramolecular motion (slow non-radiative decay rate), (iii) 3D configuration for suppressing intermolecular interactions that lead to emission self-quenching and TTA, and (iv) relatively short emission life-time (4.3–5.1 μs) which is useful to avoid excitons annihilation. Applying **5** or **6** as emitter in simple-structured OLEDs, high PEs of 118 and 126 lm W^{-1} have been achieved with the respective yellow light-emitting and green light-emitting devices. And their maximum EQE have reached 26% and 27% respectively. Fig. S34 (ESI†) depicts PL spectra of **1**–**6** doped in TCTA, which was used as the host material in OLEDs based on **1**–**6**. It is noted that at both low concentration of 2 wt% and high concentration of 10 wt%, host emission from TCTA is quite strong, indicating inefficient energy transfer from TCTA to **1**–**6**. Thus, the fact that host emission is invisible in EL spectra of **1**–**6** (Fig. 7 and Fig. 10) suggests that charge trapping could be the main mechanism accounting for the EL of OLEDs with **1**–**6** light-emitting material.

In contrast to monochromic OLED, intermolecular interactions should be moderately encouraged in using luminescent Pt(II) material for WOLED. This is because a single Pt(II) emitter can give light in both the high-energy and low-energy spectral region, the later comes from excited states of the aggregates/excimers. Complex **7** and its derivatives display both high-energy monomer emission at 480 nm and low-energy excimer emission at 620 nm with high emission quantum yields (ϕ > 0.7).[8a,9b] The excimer emission is attributed to triplet excited state with quinoidal-structure that is formed by the interactions between monomer excited state and adjacent ground state molecule.[8a] Previously, we showed efficient solution processed WPLED having balanced white light with EQE of 11.51%, CIE coordinates of (0.41, 0.45), and CRI of 74 at 1000 cd m^{-2} with the use of single emissive dopant **7** alone.[9b] In this work, we used **7** as a single emitter to fabricate white OLED. Maximum EQE of 25.1%, Max. PE of 55.5 lm W^{-1}, CIE coordinates of (0.42, 0.46) and CRI = 78 have been achieved, which are compatible to the best reported WOLED based on a single light-emitting material.

Conclusion

In summary, we have designed and prepared structurally robust, bulky phosphorescent Pt(II) complexes **1**–**6**, all of which are supported by rigid tetradentate [O^N^C^N] ligands having *tert*-butyl groups, bridging tertiary amine moiety or biphenyl spiro linkage substituent, at the periphery of the ligand scaffold. High PEs of 118 and 126 lm W^{-1} have been respectively achieved in the yellow-emitting **5** and green-emitting **6**-OLEDs. The maximum EQEs of these OLEDs have been achieved to 26% and 27%, respectively. High efficiency WOELD was fabricated with complex **7** as single emitter. The maximum EQE for this WOLED was 25.1%. This work highlights the enormous potential of phosphorescent platinum(II) materials in practical OLED technology.

Acknowledgements

We gratefully acknowledge the support from the Theme-Based Research Scheme (T23-713/11), the National Key Basic Research Program of China (No. 2013CB834802), Research Grants Council of Hong Kong SAR (HKU 700812), the National Science Foundation of China (No. 61274002), Research Grants Council of Hong Kong SAR (HKU 700812) and the Innovation and Technology Commission of the HKSAR Government (GHP/043/10). This work was also supported by Guangdong Special Project of the Introduction of Innovative R&D Teams and GuangDong Aglaia Optoelectronic Materials Co., Ltd. Dr. S. C. F. Kui acknowledges the small project funding (201309176101) and the postdoctoral fellow scholarship from The University of Hong Kong.

Notes and references

[a] State Key Laboratory of Synthetic Chemistry, HKU-CAS Joint Laboratory on New Materials, and Department of Chemistry, The University of Hong Kong, Pokfulam Road, Hong Kong SAR, China. E-mail: cmche@hku.hk
[b] State Key Laboratory on Integrated Optoelectronics, College of Electronic Science and Engineering, Jilin University, Changchun130012, China.
[c] State Key Laboratory of Luminescent Materials and Devices (South China University of Technology) and Institute of Polymer Optoelectronic Materials and Devices, South China University of Technology, Guangzhou 510640, China.
[d] HKU Shenzhen Institute of Research and Innovation, Shenzhen 518053, China.

[e] GuangDong Aglaia Optoelectronic Materials Co., Ltd.
[f] School of Chemistry and Chemical engineering, Shenzhen University, Shenzhen, Guangdong, P. R. China, 518060.

† Electronic Supplementary Information (ESI) available: Experimental procedures, X-ray crystallographic data of **6** (CCDC 894324), device performance of **1**–**6**. For ESI and crystallographic data in CIF or other electronic format see DOI: 10.1039/b000000x/

1 (*a*) C. W. Tang and S. A. VanSlyke, *Appl. Phys. Lett.*, 1987, **51**, 913; (*b*) Y. Ma, H. Zhang, J. Shen and C.-M. Che, *Synth. Met.*, 1998, **94**, 245; (*c*) M. A. Baldo, D. F. O'Brien, Y. You, A. Shoustikov, S. Sibley, M. E. Thompson and S. R. Forrest, *Nature*, 1998, **395**, 151.

2 Z. B. Wang, M. G. Helander, J. Qiu, D. P. Puzzo, M. T. Greiner, Z. M. Hudson, S. Wang, Z. W. Liu and Z. H. Lu, *Nature Photon.*, 2011, **5**, 753.

3 (*a*) M. A. Baldo, S. Lamansky, P. E. Burrows, M. E. Thompson and S. R. Forrest, *Appl. Phys. Lett.*, 1999, **75**, 4; (*b*) S. Lamansky, P. Djurovich, D. Murphy, F. Abdel-Razzaq, H.-E. Lee, C. Adachi, P. E. Burrows, S. R. Forrest and M. E. Thompson, *J. Am. Chem. Soc.*, 2001, **123**, 4304.

4 (*a*) S. Reineke, T. C. Rosenow, B. Lüssem and K. Leo, *Adv. Mater.*, 2010, **22**, 3189; (*b*) Y. Tao, Q. Wang, C. Yang, C. Zhong, J. Qin and D. Ma, *Adv. Funct. Mater.*, 2010, **20**, 2923; (*c*) D. Tanaka, H. Sasabe, Y.-J. Li, S.-J. Su, T. Takeda and J. Kido, *Jpn. J. Appl. Phys.*, 2007, **46**, L10; (*d*) H. Sasabe, H. Nakanishi, Y. Watanabe, S. Yano, M. Hirasawa, Y.-J. Pu and J. Kido, *Adv. Funct. Mater.*, 2013, **23**, 5550.

5 (*a*) R. J. Holmes, S. R. Forrest, T. Sajoto, A. Tamayo, P. I. Djurovich, M. E. Thompson, J. Brooks, Y.-J. Tung, B. W. D'Andrade, M. S. Weaver, R. C. Kwong and J. J. Brown, *Appl. Phys. Lett.*, 2005, **87**, 243507; (*b*) E. Baranoff, S. Suàrez, P. Bugnon, C. Barolo, R. Buscaino, R. Scopelliti, L. Zuppiroli, M. Graetzel and Md. K. Nazeeruddin, *Inorg. Chem.*, 2008, **47**, 6575.

6 S.-C. Chan, M. C. W. Chan, Y. Wang, C.-M. Che, K.-K. Cheung and N. Zhu, *Chem. Eur. J.*, 2001, **7**, 4180.

7 (*a*) Z. B. Wang, M. G. Helander, Z. M. Hudson, J. Qiu, S. Wang and Z. H. Lu, *Appl. Phys. Lett.*, 2011, **98**, 213301; (*b*) H. Fukagawa, T. Shimizu, H. Hanashima, Y. Osada, M. Suzuki and H. Fujikake, *Adv. Mater.*, 2012, **24**, 5099; (*c*) X.-C. Hang, T. Fleetham, E. Turner, J. Brooks and J. Li, *Angew. Chem. Int. Ed.*, 2013, **52**, 6753.

8 (*a*) S. C. F. Kui, P. K. Chow, G. S. M. Tong, S.-L. Lai, G. Cheng, C.-C. Kwok, K.-H. Low, M. Y. Ko and C.-M. Che, *Chem. Eur. J.*, 2013, **19**, 69; (*b*) S. C. F. Kui, P. K. Chow, G. Cheng, C.-C. Kwok, C. L. Kwong, K.-H. Low and C.-M. Che, *Chem. Commun.*, 2013, **49**, 1497; (*c*) S.-L. Lai, W.-Y. Tong, S. C. F. Kui, M.-Y. Chan, C.-C. Kwok and C.-M. Che, *Adv. Funct. Mater.*, 2013, **23**, 5168.

9 (*a*) T. Fleetham, J. Ecton, Z. Wang, N. Bakken and J. Li, *Adv. Mater.*, 2013, **25**, 2573; (*b*) G. Cheng, P.-K. Chow, S. C. F. Kui, C.-C. Kwok, and C.-M. Che, *Adv. Mater.*, 2013, **25**, 6765; (c) G. Li, T. Fleetham and J. Li, *Adv. Mater.*, 2014, **26**, 2931.

10 (*a*) K. Li, G. Cheng, C. S. Ma, X. G. Guan, W. M. Kwok, Y. Chen, W. Lu and C.-M. Che, *Chem. Sci.*, 2013, **4**, 2630; (*b*) L. Zhou, C.-C. Kwok, G. Cheng, H. Zhang and C.-M. Che, *Opt. Lett.*, 2013, **38**, 2373.

11 S. R. Forrest, D. D. C. Bradley and M. Thompson, *Adv. Mater.*, 2003, **15**, 1043.

12 H.-F. Xiang, S.-C. Chan, K. K.-Y. Wu, C.-M. Che and P. T. Lai, *Chem. Commun.*, 2005, 1408.

13 K. Li, X. Guan, C.-W. Ma, W. Lu, Y. Chen and C.-M. Che, *Chem. Commun.*, 2011, **47**, 9075.

14 Y.-Y. Lin, S.-C. Chan, M. C. W. Chan, Y.-J. Hou, N. Zhu, C.-M. Che, Y. Liu and Y. Wang, *Chem. Eur. J.*, 2003, **9**, 1263.

15 C.-M. Che, C.-C. Kwok, S.-W. Lai, A. F. Rausch, W. J. Finkenzeller, N. Zhu and H. Yersin, *Chem. Eur. J.*, 2010, **16**, 233.

16 (*a*) D. A. K. Vezzu, J. C. Deaton, J. S. Jones, L. Bartolotti, C. F. Harris, A. P. Marchetti, M. Kondakova, R. D. Pike and S. Huo, *Inorg. Chem.*, 2010, **49**, 5107; (*b*) D. Ravindranathan, D. A. K. Vezzu, L. Bartolotti, P. D. Boyle and S. Huo, *Inorg. Chem.*, 2010, **49**, 8922.

17 E. Turner, N. Bakken and J. Li, *Inorg. Chem.*, 2013, **52**, 7344.

18 (*a*) M. Hissler, W. B. Connick, D. K. Geiger, J. E. McGarrah, D. Lipa, R. J. Lachicotte and R. Eisenberg, *Inorg. Chem.*, 2000, **39**, 447; (*b*) Z. Abedin-Siddique, T. Ohno, K. Nozaki and T. Tsubomura, *Inorg. Chem.*, 2004, **43**, 663.

19 S.-J. Su, H. Sasabe, Y.-J. Pu, K.-I. Nakayama and J. Kido, *Adv. Mater.*, 2010, **22**, 3311.

20 C. Murawski, K. Leo and M. C. Gather, *Adv. Mater.*, 2013, **25**, 6801.

21 G. Zhou, W.-Y. Wong and X. Yang, *Chem. Asian J.*, 2011, **6**, 1706.

22 T. P. I. Saragi, T. Spehr, A. Siebert, T. Fuhrmann-Lieker and J. Salbeck, *Chem. Rev.*, 2007, **107**, 1011.

23 X.-H. Zhao, G.-H. Xie, Z.-D. Liu, W.-J. Li, M.-D. Yi, L.-H. Xie, C.-P. Hu, R. Zhu, Q. Zhao, Y. Zhao, J.-F. Zhao, Y. Qian and W. Huang *Chem. Commun.*, 2012, **48**, 3854.

24 C. Féry, B. Racine, D. Vaufrey, H. Doyeux and S. Cinà, *Appl. Phys. Lett.*, 2005, **87**, 213502.

